ISSN 0036-0244, Russian Journal of Physical Chemistry A, 2023, Vol. 97, No. 13, pp. 3089–3103. © Pleiades Publishing, Ltd., 2023.

PHYSICAL CHEMISTRY OF NANOCLUSTERS, SUPRAMOLECULAR STRUCTURES, AND NANOMATERIALS

Spectroscopic and In Silico Characterization of Irınotecan-Loaded Nanoparticles: In Vitro Evaluation for Breast Cancer Treatment

Fatmanur Ozcelik[a], Tevfik Raci Sertbakan[a], and Serap Yalcin[b,*]

[a] *Department of Physics, Faculty of Art and Sciences, Kırsehir Ahi Evran University, Kırsehir, 40100 Turkey*

[b] *Department of Medical Pharmacology, Faculty of Medicine, Kırsehir Ahi Evran University, Kırsehir, 40100 Turkey*

** e-mail: syalcin@ahievran.edu.tr*

Received January 4, 2023; revised May 15, 2023; accepted May 18, 2023

Abstract—Cancer has always posed a significant threat to human health. Chemotherapy agents used in cancer treatment can also damage normal cells. The area that attracts the most attention today is the transport of chemotherapeutic drugs and the reduction of their side effects by nanotechnological methods. While increasing the stability of drugs or proteins by using nanoparticles with nanotechnology methods, controlled drug release in the target region is also aimed. Our study, it is aimed to determine the effect of iron oxide nanoparticles coated with poly-3-hydroxybutyrate (PHB) loaded with Irinotecan, an anticancer agent, on cancerous cells. In our study, Irinotecan anticancer agent and PHB molecule drawings, molecular electrostatic potential maps, and Mulliken charges of atoms were calculated with the Gaussian 09 program, and theoretical IR spectra were drawn with the Origin85 program. Before the calculation to be made in the Gaussian 09 package program, the GaussView 5.0 package program, which serves as a utility for this program, is used. The GaussView 5.0 program makes a 3-dimensional design of a molecule and provides a visual description of the molecule's properties. At the same time, the GaussView 5.0 program visualizes the calculation outputs made by the Gaussian 09 program. The geometrical structure parameters of Irinotecan anticancer agent and PHB molecule were calculated theoretically by considering the most stable structure of the molecules, such as bond length, bond angles and angle bending, binding energies. The drug-loaded nanoparticles were completed and calculated in BIODRAW and Gaussian programs, molecular docking and dynamic analysis was performed with anti-apoptotic proteins. At the same time PHB coated nanoparticles were in situ synthesized as nanocarrier systems and loaded with the drug Irinotecan. The drug loading capacity, drug release and stability of nanoparticle were analyzed. The cytotoxicity of nanoparticle, drug and drug loaded nanoparticles were tested by XTT analyses in vitro. We analyzed the 3D drawings of the PHB molecule and the cancer drug Irinotecan with the GaussView program and optimized it with the Gaussian 09 program. Then, we created molecular electrostatic potential maps with the GaussView program to determine the binding regions of these structures. In-vitro analysis, the IC_{50} was determined on breast cancer cells. In-silico analysis, molecular docking studies have been carried out on the different classes of Irinotecan, nanoparticles and Irinotecan loaded nanoparticles the target proteins. As a result of the analysis, the Irinotecan loaded PHB coated nanoparticles has been observed to be effective against cancer and likely to be a potential drug.

Keywords: Irinotecan, PHB (polyhydroxybutyrate), breast cancer cell, vibration spectra, molecular docking, molecular dynamic

DOI: 10.1134/S0036024423130095

1. INTRODUCTION

Breast cancer is one of the most frequently diagnosed cancers in women worldwide, accounting for 16% of all female cancer cases that begin in the breast tissue, which consists of glands called lobules for milk production and the ducts that connect the lobules to the nipple. The rest of the breast consists of fat, connective, and lymph tissue. There are two types in origin, ductal and lobular, 80–90% of cases are ductal carcinoma and 10–20% are lobular carcinoma [1].

There are currently three main treatments for breast cancer: surgery, radiation, and chemotherapy. Chemotherapy is crucial for the treatment of breast cancer patients. It is well known that even the smallest molecules of chemotherapy drugs can kill cancer cells, but due to their lack of selectivity, they can also cause similar side effects and unbearable pain to normal tissues and cells. As a result, new approaches and methods for cancer treatment are urgently needed [2].

As nanotechnology develops toward the development of nanomedicine agents, therapeutic approaches against cancer may improve greatly [3]. There are many unique efficient alternatives to designing and synthesizing small-size nanomaterials that target both active and passive roles, and that can be used to attach multiple targeting moieties by controlled cellular

uptakes with a minimum amount of nanometric carriers. On the same pathway, they can carry drug, tracking-probes, and ligands, targeting each BC cell specifically. Targeted delivery of molecules with multiple specificities, tracking, diagnosing, and treating emerge as a theranostic approach [4].

There are numerous nanoparticles that are used for various purposes as a result of their different properties. These include nanoclay types, iron-based nanoparticles like magnetite (Fe_3O_4) and hematite (Fe_2O_3), cubic boron nitride, polytetrafluoroethylene (PTFE), nano silver, titanium dioxide, magnesium oxide, and fullerene [5].

We used magnetic nanoparticles in this study. Magnetic nanoparticles, a class of nanoparticles that can be manipulated using magnetic fields, usually consist of a magnetic material (such as iron, nickel, cobalt) and a chemical component with functionality [6].

The use of MNPs has increased in many medical applications such as controlled drug release, biosensing, magnetic resonance imaging (MRI), and hyperthermia cancer therapy [7]. When further "functionalized" with drugs and bioactive agents, such as peptides and nucleic acids, MNPs form distinct particulate systems that penetrate cell and tissue barriers and offer organ-specific therapeutic and diagnostic modalities [8].

Additionally, in vivo magnetic properties and MNP activity can be customized by applying a safe and biocompatible coating to increase their acceptability for a particular target in the human body. This coating provides surface chemistry that aids in the integration of functional ligands. The result of altering the surface chemistry may be the multifunctionality of MNPs [7].

In our study, we chose poly-3-hydroxybutyrate (PHB) as the biocompatible coating and coated MNPs with this polymer. The most widely used members of this biopolymer group are PHB and its hydroxyvalerate (PHB-HV) copolymers. They are produced biosynthetically from natural raw materials by bacteria and can be easily degraded by microorganisms under different conditions [9].

PHB is a fully biodegradable semi-crystalline thermoplastic that is biocompatible and non-toxic, obtained from renewable resources through a low-impact biotechnological process, thermally degraded around its melting temperature [10].

It is one of the synthetic polymers often used to cover MNPs. It gives the MNPs a hydrophilic surface and minimizes their agglomeration. Thus, PEG coating increases the circulation time of MNPs by reducing their phagocytosis by macrophages [11].

In this study, newly synthesized PHB-coated MNPs (PHB-MNPs) with targeting potential under magnetic field were characterized by FTIR and TEM analyses. Loading efficiencies and drug releases at different pHs were investigated after Irinotecan loading to PHB-MNPs. In addition, in vitro cytotoxicity analysis of Irinotecan-loaded PHB-MNPs on the Irinotecan-resistant Michigan Cancer Foundation-7 (human breast adenocarcinoma) MCF-7 cell line. At the same time, binding energies to anti-apoptotic proteins were calculated with this system molecular docking analysis.

lrinotecan (CPT-11) is a semisynthetic derivative of the plant (*Camptotheca acuminata*)-derived compound camptothecin. Camptothecin and its analogues/derivatives appear to exert their antitumour activity by binding to topoisomerase I. This enzyme catalyzes the cleavage and reclosing of supercoiled DNA, which are essential steps in DNA replication and transcription. It is the binding of camptothecin to topoisomerase I that prevents its release from DNA. Progressive replication enzymes collide with the camptothecin-topoisomerase 1-DNA complex, causing double-stranded DNA breaks that can lead to cell death. This cytotoxic activity is time-dependent and is specific to the S phase of the cell cycle. Irinotecan has demonstrated antitumor activity in vitro and in vivo carcinoma models, including colorectal, ovarian, non-small cell lung, and breast cancer [12].

In this study, quantum chemical calculations were made using the Gaussian 09 package program of PHB, Irinotecan, and the bound structure of these molecules. Vibration frequencies are calculated at the same theory level. These frequencies were calculated and scaled, and then the values were compared with the experimental infrared spectra. Vibration modes were determined as based on TED analysis using the SQM program on the basis of 6*p*311++G(*d,p*) for PHB molecule, 6-31G for Irinotecan, and 6-31G(*d,p*) for bound structure. In addition, molecular electrostatic potential (MEP) maps of the investigated molecule were made using the DFT method.

2. MATERIALS AND METHODS

2.1. 2D Development of MCF-7 Cell Line

Cancer cell lines were grown in 75 cm^2 flasks in 88% RPMI-1640 medium supplemented with 10% Fetal Bovine Serum and 1% Gentamicin and 1% Penicillin antibiotic at 37°C and 5% carbon dioxide incubator. Cells were passaged using trypsin, as 80% of the flask surface was covered by cells.

2.2. Cytotoxicity Analysis in Breast Cancer Cell Cultures

Cytotoxicity analysis was performed to determine the cytotoxic effects of free drug and drug-loaded nanoparticles on cells grown in cell cultures, and to determine the dose of the drug to be administered to the cells. Cytotoxicity of MCF-7 cells was performed using an XTT-based cytotoxicity analysis kit. Cells were seeded into 96-well plates at 5000 cells per well. One column of the plate is reserved as the medium

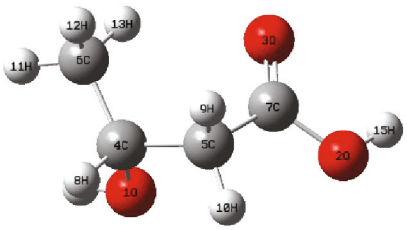

Fig. 1. Poly-3-hydroxybutyrate (PHB).

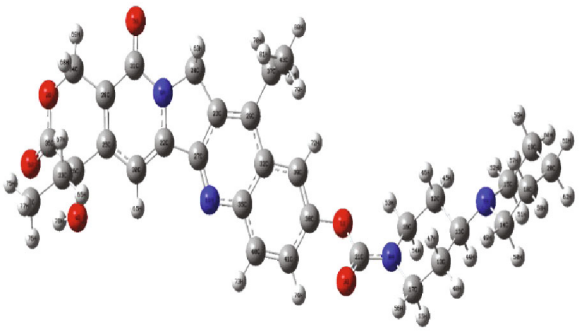

Fig. 2. Irinotecan.

control and no cells are seeded there. After a while, the relevant drug was given to the wells in serial dilutions, and after 48 to 72 h, XTT chemical with formazan dye was added to each well and left in the incubator for 2 to 5 h, and optical densities were calculated using an ELISA reader. 100% growth was assumed in untreated wells and growth in wells containing different amounts of drug was determined by proportioning it. Finally, the growth rate corresponding to each drug concentration was determined. Each sample was performed in at least three replicates.

2.3. Irinotecan Loading on Magnetic Nanoparticles

Loading studies of the drug into magnetic nanoparticles were performed in PBS (pH 7.2), TES (pH 7.3), and acetate (pH 5.0) buffers. Parameters such as mixing speed, vibration frequency and duration were optimized in the drug rotator device to be prepared at different concentrations. Then, drug-loaded nanoparticles were separated by the magnetic separation method. By taking the supernatant, absorbance will be measured in UV spectrophotometer and the amount of drug binding to nanoparticles was determined.

2.4. Characterization of Drug-Loaded Nanoparticles

Particle shapes and sizes were observed at every stage of the synthesis of drug-loaded nanoparticles by electron microscopy (SEM). In addition, the characterization of Irinotecan loaded. Nanoparticles was done by FTIR analysis.

2.5. Release of Drug Nanoparticles

The release of the drug was analyzed in acetate buffer prepared at two different pHs (pH 5.2 and 4.2) in accordance with intracellular and endosomal pH. The amount of release of the drug was determined by measuring the absorbance in the solution in a UV spectrophotometer.

2.6. Drawing Molecules and Calculating Their Energies

PHB and Irinotecan molecule were purchased from Sigma-Aldrich. The FT-IR spectra of the molecules were taken using the Perkin-Elmer Spectrum One FT-IR spectrometer at room temperature in the region of 4000–400 cm^{-1} with the pellet method in the KBr window. Raman spectrum of Irinotecan molecule was taken using Thermo Scientific DXR Raman microscope with Nd:YVO_4 DPSS Raman spectrophotometer excited with 532 nm laser in the 4000–50 cm^{-1} region.

In this study, we optimized PHB, Irinotecan and bound PHB and Irinotecan molecules with the Gaussian 09 package program. While doing this, base sets of 6-311++G(*d*,*p*), 6-31G(*d*), and cc-pVDZ with the DFT(B3LYP) method for PHB molecule, and 6-31G with the DFT(B3LYP) method for the Irinotecan molecule. We used 31G(*d*,*p*) and cc-pVDZ base sets, and 6-31G base sets for the bound PHB and Irinotecan molecule. The shapes of these molecules as a result of geometric optimization are given in Figs. 1–3. Geometric parameters of molecules such as bond lengths, bond angles, and dihedral angles were calculated using Density Functional Theory (DFT) with various basis sets at the B3LYP level [13]. Using the same method and basis sets as in DFT, the vibrational frequencies of the molecules were calculated and then multiplied by the scale factors and presented in a tabular form. In addition, vibration modes were assigned by TED analysis using the Gaussian 09 program [14]. These vibration frequencies obtained were compared with their experimental values. Molecular electrostatic potential is related to electron density and is a very useful descriptor for our understanding of hydrogen bond interactions. MEP maps of molecules were drawn with the same method and base set [15].

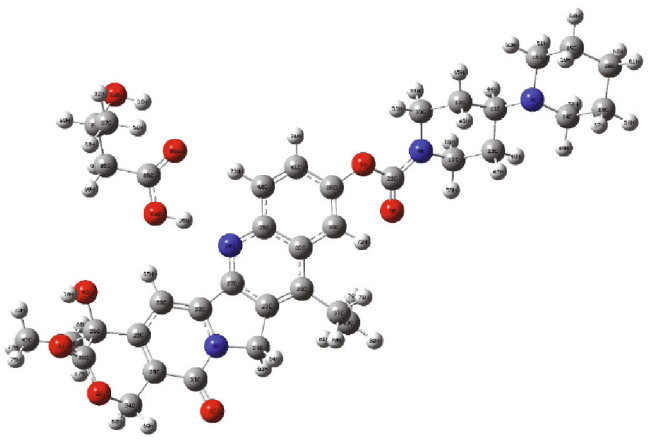

Fig. 3. Bound Irinotecan and PHB molecule.

2.7. Molecular Docking Analysis

The complete molecular structure of the molecule for ligand preparation was drawn using Gaussian 09. The intended crystal protein structures were retrieved from the protein data bank (www.rcsb.org) (BCL-2 PDB ID: 4MAN, BCL-W PDB ID: 2Y6W, MCl-1 PDB ID: 5FDO; AKT-1 PDB ID: 4gv1, BRAF PDB ID: 5vam). Molecular docking calculations were performed with the Lamarckian Generic Algorithm in Autodock Vina [16, 17]. All bound water molecules and ligands were removed from proteins, non-polar hydrogen atoms were merged and polar hydrogen atoms were added. BIOVIA was used to visualize the protein as a ligand [18].

2.8. Molecular Dynamics (MD) Simulation Analysis

Simulation of the ligand and protein complex was performed using WebGro free software. MD simulation was performed for 50 ns to check the stability between the ligand and protein complex (WebGro, 2021) [13, 19].

3. RESULTS AND DISCUSSION

In this study, Irinotecan loaded PHB coated magnetic nanoparticles were synthesized to be used in the treatment of cancers with targeted drug release. PHB coated superparamagnetic iron oxide nanoparticles were synthesized by simultaneous in situ precipitation method. Characterization of nanoparticles was performed by XRD, XPS/ESCA, FTIR, TEM, DLS, TGA, VSM, and zeta potential analyzes [1]. The characterization of PHB, Irinotecan molecules, and the combined form of these molecules, PHB–Irinotecan, were performed with FTIR, TEM, TGA, and VSM analyses [2]. FTIR spectra of these structures were analyzed using the solid state KBr disk method. These spectra were recorded in the range of 4000–400 cm^{-1} at room temperature with the Thermo Scientific Nicolet 6700 FT-IR device in Kırşehir Ahi Evran University Central Research and Application Laboratory. Experimental and theoretical FTIR spectra of pure PHB molecule, Irinotecan drug and bound PHB–Irinotecan structure were drawn (Figs. 4–6). These spectra are in agreement both experimentally and theoretically. As a result of the interpretation of these spectra, it can be concluded that PHB-MNPs form their structure [14, 20].

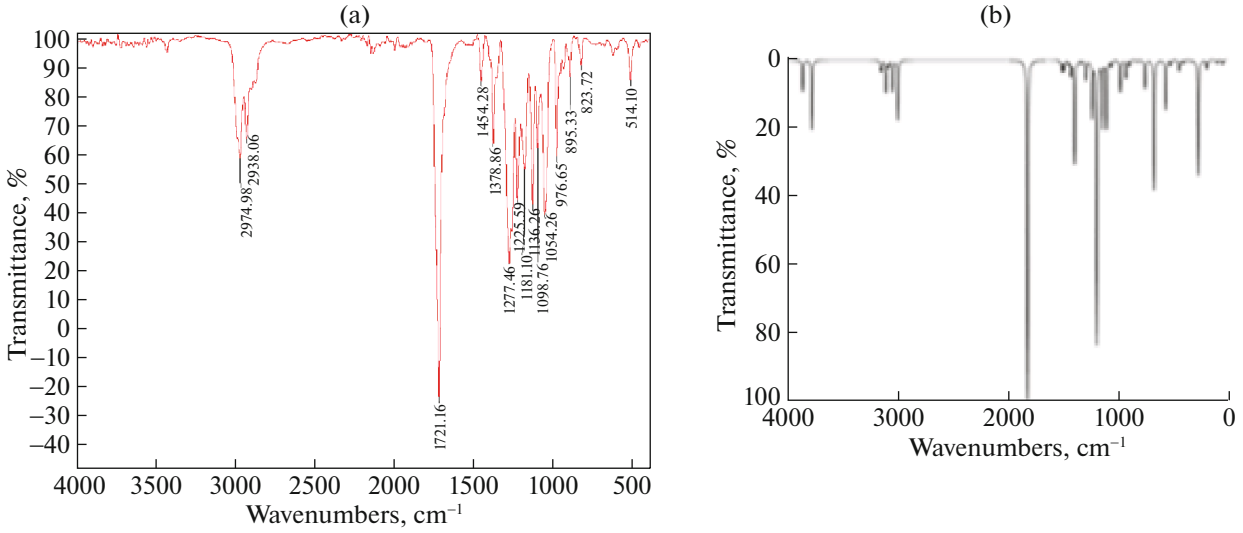

Fig. 4. Experimental (a) and theoretical (B3LYP/6-311++G(*d,p*) (b), FT–IR spectra of PHB molecule, respectively.

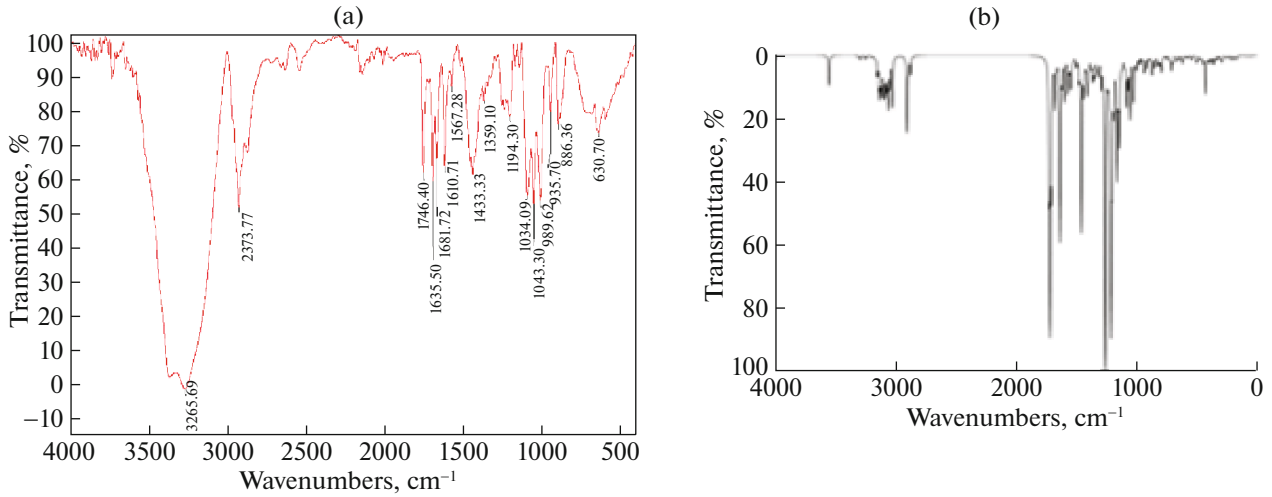

Fig. 5. Experimental (a) and theoretical (B3LYP/6-31G) (b), FT-IR spectra of Irinotecan molecule, respectively.

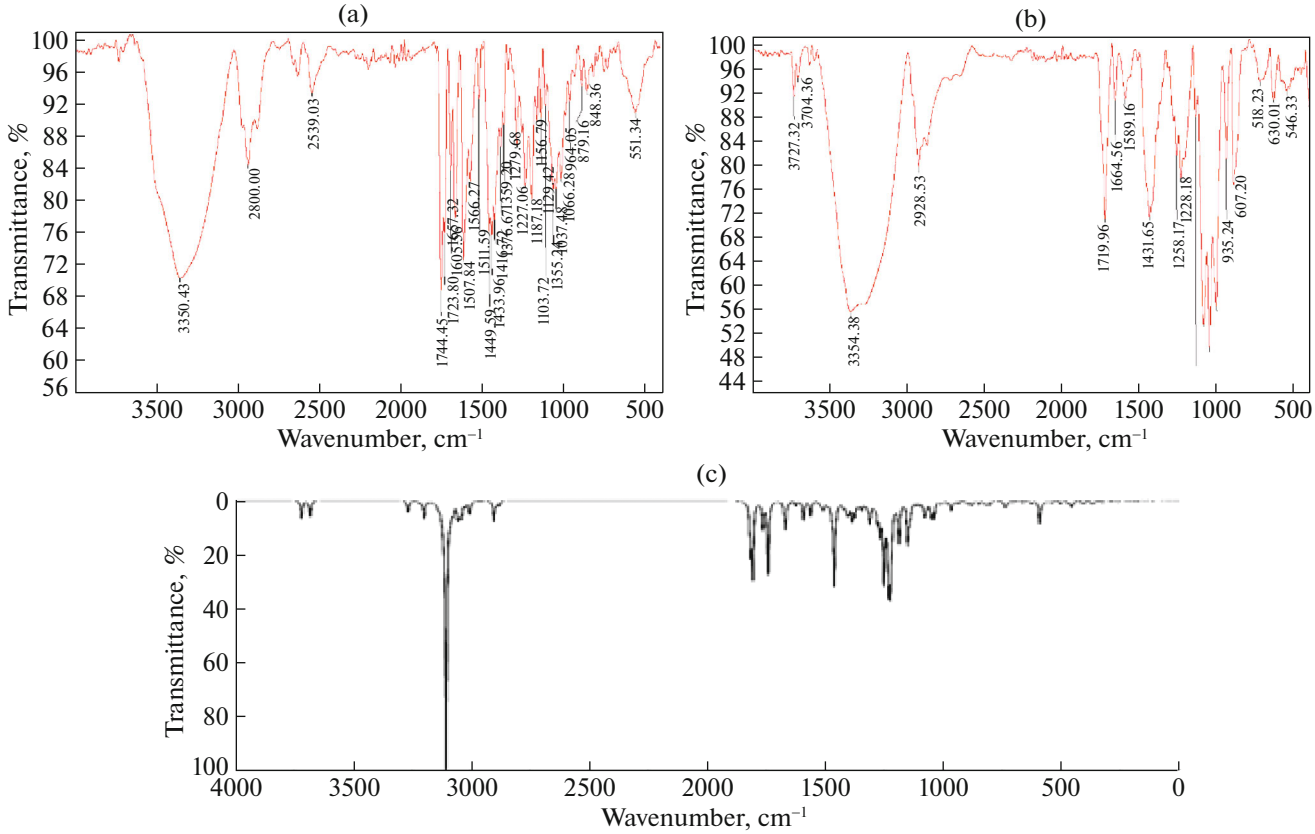

Fig. 6. Experimental (a) 30 and (b) 200 μL and theoretical (c) B3LYP/6-31G (base sets) FT-IR spectra of bound Irinotecan and PHB molecule, respectively.

3.1. Geometric Parameters of Molecules

In our study, we calculated Irinotecan anticancer agent and PHB molecule drawings and MEP maps with the Gaussian 09 program. We drew the theoretical IR spectra with the Origin85 program. Before the calculation to be made in the Gaussian 09 package program, we used the GaussView 5.0 package program, which serves as a utility for this program.

As a result of geometric optimization of any gaseous molecule, the lowest energy most stable state of the molecule is found. Optimized versions of the molecules used; 6-311++G(*d*,*p*), 6-31 G(*d*), and cc-pVDZ base

sets for PHB by DFT(B3LYP) method, 6-31 G, 6-31 G(*d*,*p*), cc-pVDZ base sets and finally for the Irinotecan and bonded structure were obtained by DFT(B3LYP) method using 6-31 G(*d*,*p*) base set. Interatomic bond lengths and angles between bonds of PHB, Irinotecan, and PHB–Irinotecan bonded structures were found by using the most stable state forms. The results are shown in Table 1.

As a result of the calculation, it was observed that the bond length values of Irinotecan and PHB molecules were compatible with the literature and did not show much difference after binding, and hydrogen bonding was established between N_{10}–H_{96}, O_4–H_{90}, and H_{65}–O_{83} atoms.

3.2. Vibrational Assignments

Spectroscopic study of Irinotecan molecule was done by Babu et al. [21]. Here, we accepted this study as a reference study and made comparisons.

The Irinotecan molecule consists of 81 atoms, so it has 237 vibrational normal modes. The entire Irinotecan molecule consists of two different groups, which are ethyl-substituted camptothecin and bipiperidine ester. Ethyl-substituted camptothecin consists of five rings, four of which are six-membered and one is five-membered rings. The piperidine ring is in chair conformation with the endocyclic bond angle close to the tetrahedral geometry [21].

In the Ethyl-substituted camptothecin part of the molecule, C–H stretching vibrations were found at DFT-B3LYP level as 3152, 3142, 3104, 3089, 3058, and 3042 cm^{-1} in the reference article, and as 3042, 3046, 3069, 3107, 3163, 3177 in our study. C–H stretching vibrations show their presence in the characteristic region of the spectrum, 3100–3000 cm^{-1} [22, 23].

The carbon–carbon stress modes of the phenyl group are expected to be in the range of 1650 to 1200 cm^{-1}. The actual location of these modes is determined by the form of substitution around the ring rather than the nature of the substituents [24]. C=C vibrations calculated theoretically in the reference article are in the range of 1674–1504 and 1437–1428 cm^{-1}, whereas in our study, they are in the range of 1640–1509 and 1441–1423 cm^{-1} and are consistent with the experimental values.

The fundamental vibration modes of the PHB molecule, on the other hand, were investigated considering the group frequencies of CH_2 (methylene), CH_3 (methyl), O=C and O–H stretching and bending vibrations. The stretching vibrations of the methylene groups are found in a very complex band spread over a region of 2800–3000 cm^{-1} [25].

Table 1. Some bond length values of PHB, Irinotecan, and bound PHB–Irinotecan molecules

Parameters	Theoretical (B3LYP) 6-31G(*d*,*p*)		
	PHB–Irinotecan	Irinotecan	PHB
	Bond lengths, Å		
O_4–H_{90}	3.8085		
N_{10}–H_{96}	1.7953		
H_{65}–O_{83}	2.2608		
N_7–C_{11}	1.4772	1.4771	
N_7–C_{14}	1.4691	1.4693	
N_7–C_{15}	1.4705	1.4708	
N_8–C_{16}	1.4635	1.4623	
N_8–C_{17}	1.4618	1.4608	
N_8–C_{21}	1.3589	1.3597	
N_9–C_{22}	1.3805	1.3776	
N_9–C_{24}	1.4666	1.4702	
N_9–C_{31}	1.3975	1.3979	
N_{10}–C_{27}	1.3201	1.3136	
N_{10}–C_{35}	1.3695	1.3637	
O_{82}–C_{85}	1.4202		1.4279
O_{82}–H_{95}	0.9722		0.9660
O_{83}–C_{88}	1.3283		1.3532
O_{83}–H_{96}	1.0045		0.9727
O_{84}–C_{88}	1.2272		1.2129
C_{85}–C_{86}	1.5428		1.5373
C_{85}–C_{87}	1.5329		1.5284
C_{85}–H_{89}	1.0968		1.1031
C_{86}–C_{88}	1.5157		1.5164
C_{86}–H_{90}	1.0942		1.0956
C_{86}–H_{91}	1.0976		1.0916
C_{87}–H_{92}	1.0933		1.0970
C_{87}–H_{93}	1.0958		1.0951
C_{87}–H_{94}	1.0947		1.0910

Table 2. Vibration frequencies of bound Irinotecan and PHB molecule

Theoretical (B3LYP)			Experimental		TED, %
6-31G(*d*,*p*)			C	D	
normal modes	freq.[a]	I_{IR}^{b}			
ν_{282}	3573	126.14	3745 vw	3727 w	ν_{OH} (77)
ν_{281}	3538	113.21	3658 vw	3704 wv	ν_{OH} (79)
ν_{280}	3150	1.06		3296 vs	ν_{CH} (70)
ν_{279}	3140	81.56	3350 vs	3364 vs	ν_{CH} (33) + ν_{HO} (27)
ν_{263}	2986	1774.75	2989 m		ν_{NH} (21)+ ν_{CH} (12) + ν_{OH} (26)
ν_{260}	2973	7.48	2974 m		ν_{CH} (62)
ν_{248}	2931	13.93	2930 m		ν_{CH} (66)
ν_{245}	2923	26.86		2924 m	ν_{CH} (65)
ν_{241}	2890	79.46	2891 m		ν_{CH} (58)
ν_{240}	2887	15.77		2887 m	ν_{CH} (60)
ν_{237}	2767	28.62	2539 w		ν_{CH} (50)
ν_{236}	1746	338.33	1744 vs		ν_{OC} (22) + δ_{OCC}(12)
ν_{235}	1737	512.78	1724 vs	1720 s	ν_{OC} (19)
ν_{234}	1695	194.54	1686 m		ν_{OC} (14)
ν_{233}	1674	513.70	1658 s	1655 w	ν_{OC} (12) + ν_{CC} (16) + δ_{CCC}(11)
ν_{231}	1604	184.10	1608 vs		ν_{CC} (19) + δ_{CCC}(14) + δ_{CCH} (10)
ν_{230}	1590	6.99		1589 w	ν_{CC} (35) + δ_{CCC}(16) + δ_{CCH} (12)
ν_{229}	1562	32.56	1565 m		ν_{CC} (23) + δ_{CCC}(16) + δ_{CCH} (11)
ν_{227}	1501	107.78	1511 w		ν_{CC} (14) + δ_{CCH} (19)
ν_{215}	1450	22.01	1449 s		δ_{HCH} (18) + τ_{HCCH} (13) + τ_{CCCH} (12) + τ_{HCCO} (13)
ν_{209}	1434	20.09	1433 vs	1432 s	τ_{CCCH} (10) + τ_{HCCH} (15)
ν_{204}	1415	49.43	1416 s		δ_{CCH} (10) + τ_{HCCH} (8)
ν_{199}	1382	3.58	1379 m		δ_{CCH} (19) + τ_{CNCH} (15) + τ_{CCCH} (11) + τ_{HCCH} (16)
ν_{193}	1357	29.15	1359 m		δ_{CCH} (21) + τ_{CNCH} (12) + τ_{CCCH} (10) + τ_{HCCH} (16)
ν_{175}	1280	8.70	1279 m		δ_{CCH} (16) + τ_{HCCH} (21)
ν_{170}	1257	49.13		1256 m	δ_{CCH} (18) + τ_{CCCH} (10)
ν_{166}	1229	127.93		1229 s	ν_{CC} (8) + δ_{CCH} (16)
ν_{165}	1222	7.16	1227 m		δ_{CCH} (10)
ν_{159}	1184	506.27	1187 m		δ_{CCH} (12)
ν_{155}	1157	24.20	1156 w		δ_{CCH} (11)
ν_{149}	1133	3.09	1129 w	1134 m	δ_{CCH} (17) + τ_{CCCH} (13) + τ_{HCCH} (25)

Table 2. (Contd.)

Theoretical (B3LYP)			Experimental		TED, %
6-31G(*d*,*p*)			C	D	
normal modes	freq.[a]	I_{IR}^{b}			
ν_{148}	1107	286.82	1103 w		δ_{CCH} (11) + τ_{HCCH} (20)
ν_{143}	1089	9.16		1083 vs	δ_{CCH} (11)+ τ_{HCCH} (26)
ν_{141}	1068	13.64	1055 m		δ_{CCH} (13) + τ_{HCCO} (13) + τ_{CCCH} (11) + τ_{HCCH} (11)
ν_{137}	1039	52.92	1037 m	1044v s	δ_{CCH} (13)+ τ_{HCCH} (16)
ν_{130}	999	114.78	1006 m	1000 vs	δ_{CCH} (11) + τ_{CNCH} (11) + τ_{CCCH} (14) + τ_{HCCH} (13)
ν_{123}	957	3.15	954 w		δ_{CCH} (11) + τ_{HCCH} (13)
ν_{119}	934	8.54		936 m	δ_{CCH} (14) + τ_{HCCO} (14)
ν_{114}	885	0.33	879 w	887 s	δ_{CCH} (12) + τ_{CNCH} (11) + τ_{HCCH} (17)
ν_{108}	845	14.08	848 w		δ_{CCH} (12) + τ_{CNCH} (12) + τ_{HCCH} (21)
ν_{97}	773	26.75	768 vw		τ_{CNCH} (13) + τ_{CCCH} (12) + τ_{HCCH} (22)
ν_{91}	711	38.82		719 w	τ_{OCCH} (9) + τ_{HCCH} (7)
ν_{83}	635	6.75		630 w	τ_{CCCC} (16) + τ_{CCCH} (9)
ν_{75}	556	11.30	551 w	546 w	τ_{HCCO} (10) + τ_{CNHO} (9)
ν_{65}	453	12.00	455 vw		τ_{HCCH} (8) + τ_{HCCC} (6) + τ_{CCCC} (6) + τ_{CCOH} (6)

vs: very strong, s: strong, m: medium strong, w: weak, mw: medium weak, vw: very weak, ν: stretching, τ: torsion, γ: out of plane stretching, δ: in plane bending.

[a] The harmonic vibration wavenumber calculated for the B3LYP/6-31G(*d*,*p*) basis set was scaled to 0.962 factors.

[b] Infrared intensities were calculated by normalizing the highest intensity value to 100.

C: 50 μL Irinotecan was loaded on the PHB molecule.

D: 200 μL Irinotecan loaded on the PHB molecule.

The asymmetric and symmetrical stretching vibrations of the CH_2 group were calculated as 2877, 2959, and 3017 cm^{-1}, respectively, in the theoretical spectrum.

Symmetrical and asymmetrical stretching vibrations of the CH_3 group are generally observed in the wavenumber region of 2800–3000 cm^{-1} [25]. In the experimental spectrum of PHB, the CH_3 symmetrical stretching vibration mode of the methyl group was plotted at 2933 cm^{-1}, while it was calculated as 2924 cm^{-1} in the theoretical spectrum and 2980 cm^{-1} in the theoretical spectrum, which was marked at 2975 cm^{-1} in the experimental spectrum. The CH_3 asymmetric stretch vibration mode calculated at 3026 cm^{-1} in the theoretical spectrum could not be marked in the experimental spectrum screened by other C–H modes in this region.

The ν(C=O) stretch band is observed in the region of 1870–1540 cm^{-1} depending on the physical state of the molecule, the electronic effects of neighboring locations, conjugation, intramolecular and intermolecular hydrogen bonding [26]. C–O stretching vibration mode of PHB is marked at 1721 cm^{-1} in the experimental spectrum, while it is calculated as 1744 cm^{-1} in the theoretical spectrum.

The vibration assignment tables of these two molecules are not given because they are too long, only some vibrational assignments of the bonded structure are given in Table 2.

In addition, the presence of N–H stretching vibration in the 263rd mode in Table 2 supported the existence of the hydrogen bond formed.

3.3. Molecular Electrostatic Potential Maps

The MEP maps technique helps to predict the reactivity of point charges close to organic molecules, the regions that are most likely to approach these molecules, predict how different geometries can interact and form connections. Thus, these maps offer a solu-

Table 3. Results of the PHB EDX spectrum

Element	wt %	at %	Net int.	Error, %
O*K*	19.93	44.93	325.58	7.39
Na*K*	3.14	4.93	21.38	19.89
Cl*K*	1.22	1.24	38.99	10.16
Fe*K*	75.7	48.89	956.65	2.36

Table 4. Result of PHB–Irinotecan EDX spectrum

Element	wt %	at %	Net Int.	Error, %
O*K*	20.37	45.96	283.04	7.6
Na*K*	1.9	2.99	11.26	28.87
Cl*K*	2.18	2.22	60.96	9.68
Fe*K*	75.55	48.84	833.86	2.41

tion to the interpretation of interactions between the molecule of interest and other molecules [27]. In MEP maps, positive regions (blue) are associated with nucleophilic reactivity and negative regions (red) are associated with electrophilic reactivity. The regions shown in red, blue and green represent the negative, positive and zero electrostatic potential regions on the maps, respectively. The negative electrostatic potential (red) corresponds to the attraction of the proton by the total electron density of the molecule, and the positive electrostatic potential (blue) corresponds to the proton being repelled by the atomic nucleus [28].

In this study, we displayed MEP maps with GaussView 05 program to find the binding points of PHB and Irinotecan molecules (Figs. 7, 8). Thanks to the MEP maps, we identified various attachment points. From the determined points, we predicted that the lowest energy conformation is between N_{10}–H_{96} atoms and that molecules will bond between these atoms.

3.4. SEM Observations and EDX Results

The size and morphology of the synthesized PHB-MNPs were observed by SEM and EDX (Figs. 9–12). Since the characteristic X-rays have specific energy corresponding to each element, the element can be identified from the peak energy and the content of the element in the compound can be analyzed from the integrated intensity of the peak [29].

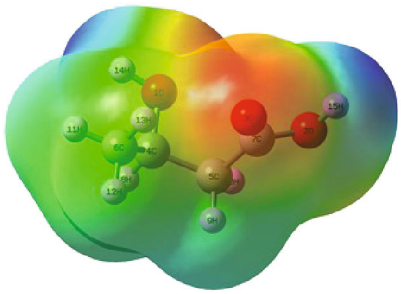

Fig. 7. MEP map of the PHB molecule.

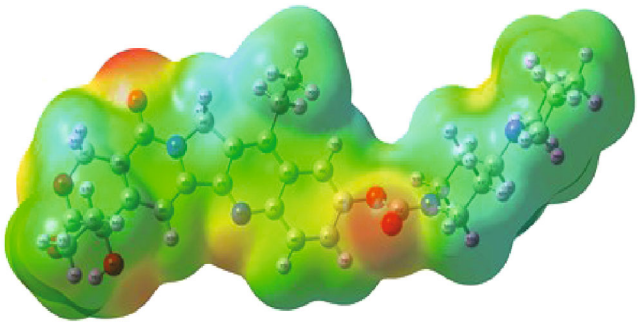

Fig. 8. Irinotecan molecule MEP map.

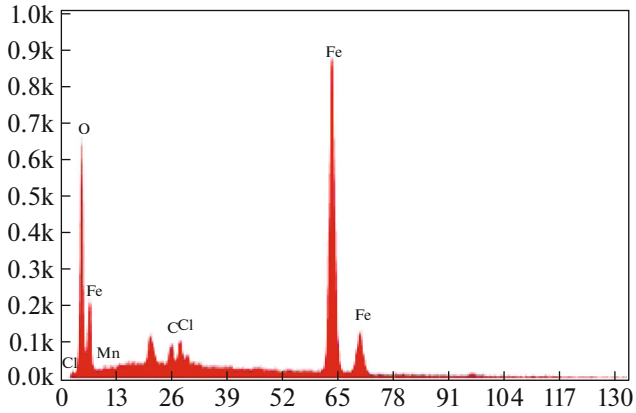

Fig. 9. PHB EDX spectrum.

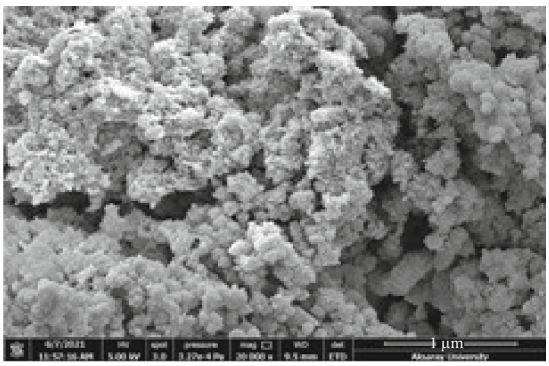

Fig. 10. SEM image of PHB.

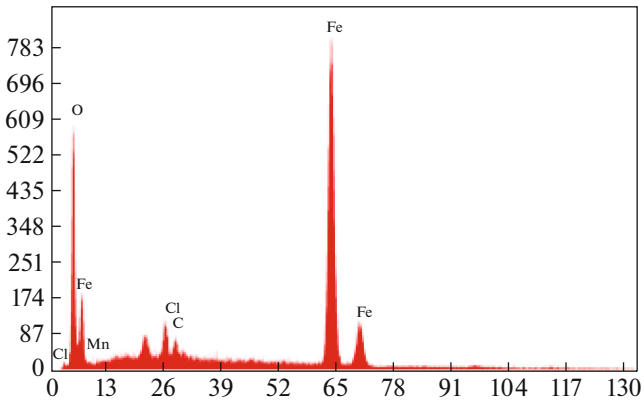

Fig. 11. PHB–Irinotecan EDX spectrum.

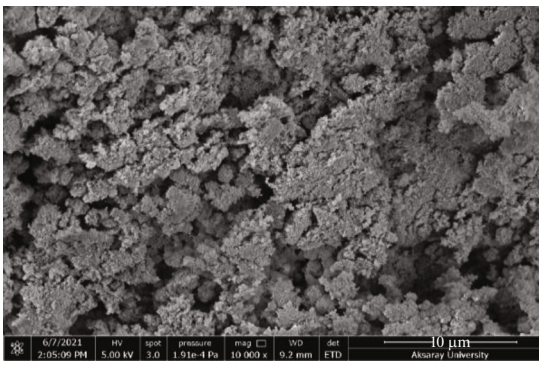

Fig. 12. SEM image of PHB–Irinotecan.

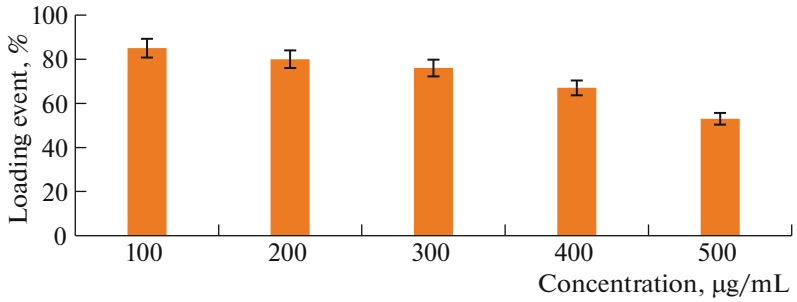

Fig. 13. Irinotecan loading graph.

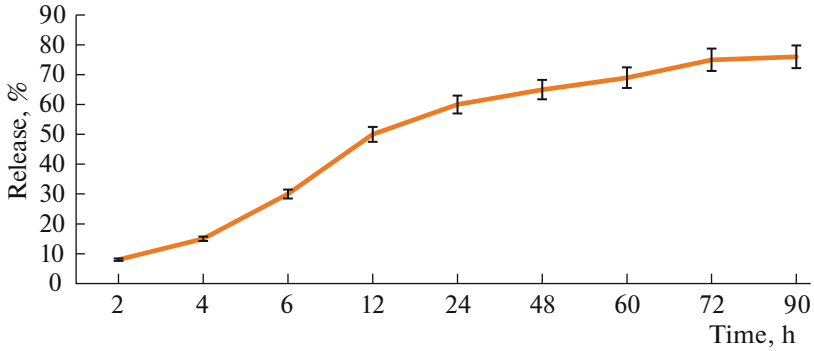

Fig. 14. Graph of drug release of PHB MNPs.

The EDX spectrum results of PHB and PHB–Irinotecan are given in Tables 3 and 4.

3.5. XTT Assay

To find the most efficient drug loading capacity on PHB-MNPs, the Irinotecan concentration was gradually increased to 500 µg/mL, where the loading efficiency began to decline. The most efficient drug loading concentration was found to be 200 µg/mL (Fig. 13).

The release studies of the most efficiently loaded concentrations were continued for up to 90 h. Approximately 60% of the drug is released from the 200 µg/mL drug loaded nanoparticles within 24 h (Fig. 14).

The cytotoxic effects of the drug on MCF-7 breast cancer cell lines were investigated with the XTT cell proliferation kit. As a result of the calculated values, IC50: 31.64 µM was found (Fig. 15).

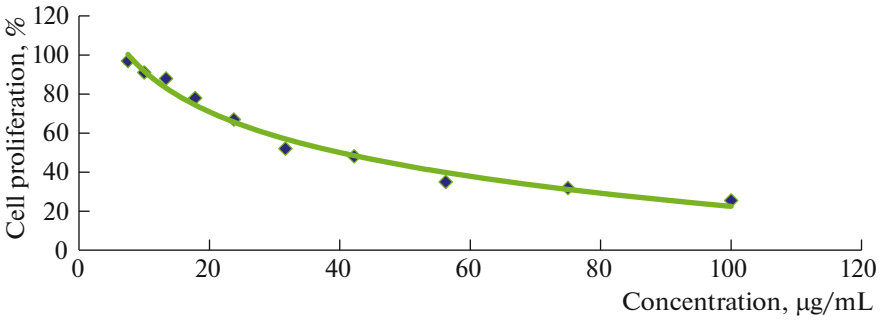

Fig. 15. Irinotecan toxicity analyses.

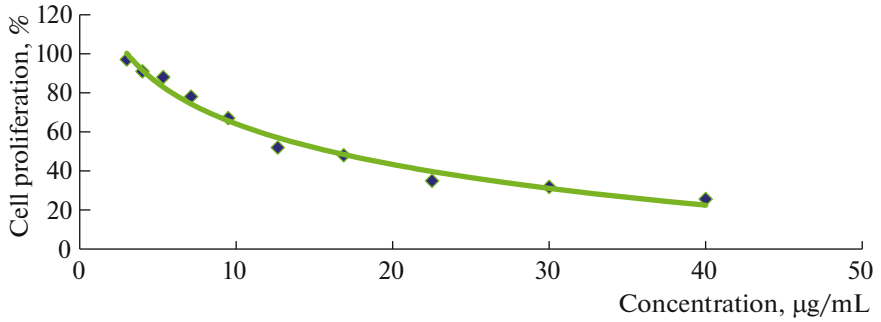

Fig. 16. Irinotecan loaded PHB-MNPs toxicity analyses.

The toxicity of drug-loaded PHB nanoparticles was found to have an IC50 value of 12.65 μM (Fig. 16).

It has been shown in our previous study that empty PHB coated nanoparticles do not have any toxicity at high doses [20].

The entry (internalization) of drug-loaded nanoparticles into cells was demonstrated under the microscope (Fig. 17).

3.6. Molecular Docking Study

Loading drugs on nanoparticles not only protects the drug, but also increases the cytotoxic effect by providing continuous release of the drug in the cytoplasm. The effectiveness of drug-loaded nanoparticles is very important because it depends on the intracellular uptake, intracellular distribution, and the dose released from the nanoparticles entering the cell.

Table 5. Binding energy results of Irinotecan molecule with anti-apoptotic proteins

Protein	Ligand	Energy values, kcal/mol
BCL-2	Irinotecan	−10.5
BCL-w	Irinotecan	−11.6
AKT-1	Irinotecan	−10.8
BRAF	Irinotecan	−11.9
MCL-1	Irinotecan	−10.7

The insertion process includes the binding conformation of the target ligand structure to the predicted protein's active site and the prediction of interactions during binding. For the docking process, a receptor and a ligand with a known 3D structure are needed. The program, on the other hand, places the ligand in the targeted region of the studied protein, starting from the 3D structures, and provides the energy and the necessary information during this time [16, 30].

The binding energy results of irinotecan molecule and drug-loaded nanoparticle molecule with anti-apoptotic proteins are given in Tables 5 and 6. In addition, the interaction of the molecule with the AKT-1 protein in Fig. 18, BRAF protein in Fig. 19, Bcl-w protein in Fig. 20, and MCL-1 protein in Fig. 21 are shown.

3.7. Molecular Dynamics Simulation Study

One of the most important criteria obtained by molecular dynamics simulation studies in the interpretation of protein and ligand interaction is root mean square deviation (RMSD) plots. A ligand that is strongly bound to the protein will have inhibited the protein's functioning. This result causes less and stable peaks to be seen in RMSD charts.

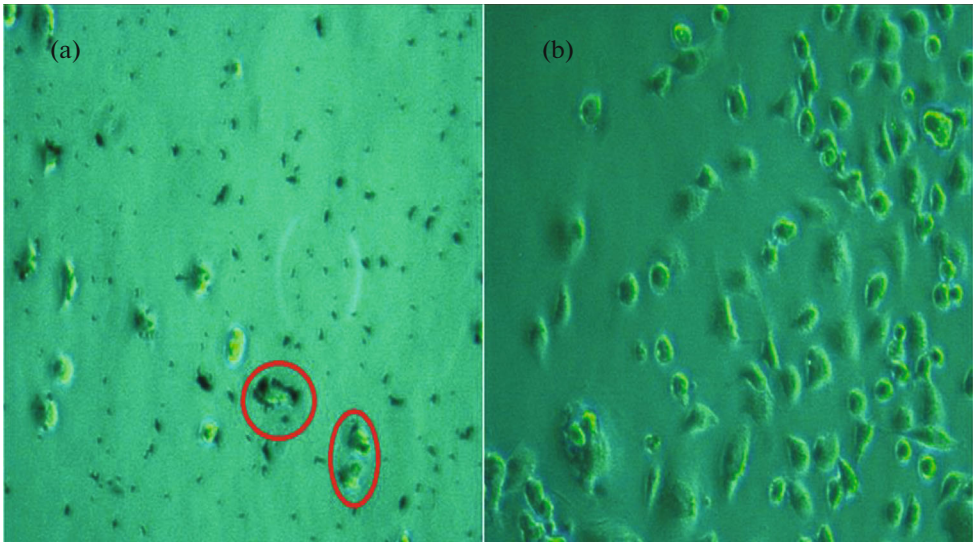

Fig. 17. Internalization of Irinotecan loaded nanoparticles into the cell ((a) Irinotecan loaded nanoparticle treated cancer cell line; (b) MCF-7 control cell line).

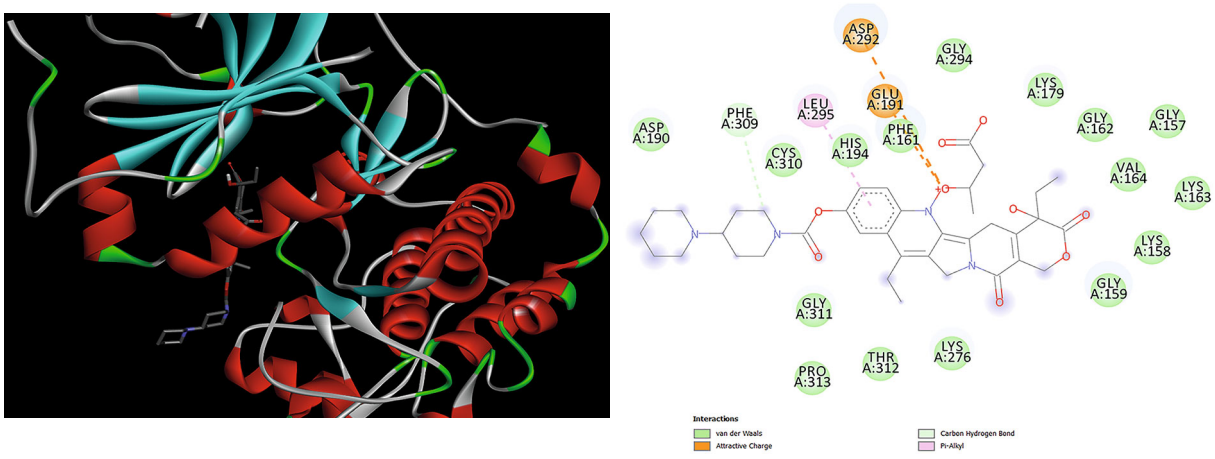

Fig. 18. Interaction of AKT-1 protein and molecule.

Table 6. Docking energy of drug-loaded nanoparticle molecule with anti-apoptotic proteins

Protein	Ligand	Energy values, kcal/mol
BCL-2	PHB–Irinotecan nanoparticle	–10.7
BCL-w	PHB–Irinotecan nanoparticle	–11.8
AKT-1	PHB–Irinotecan nanoparticle	–12.5
BRAF	PHB–Irinotecan nanoparticle	–11.5
MCL-1	PHB–Irinotecan nanoparticle	–11.3

A crucial parameter for analyzing the stability of MD trajectories, RMSD is used for the prediction of backbone atoms of protein and ligand-protein complexes. Measurements of the spine RMSD for the complex gave insight into conformational stability [31–34].

RMSF plots showed residue-to-residue variation throughout the simulation. In case of complex, all of the residues located within the C-terminal and N-terminal domains had RMSF values <5 Å, the complex formed stable and rigid conformation in the substrate binding site of the protein. The molecule and AKT-1 had hydrogen bonds in the range of 200–250. Based on the counts of hydrogen bonds that occurred during the molecular dynamics simulations, all ligands occupied the corresponding active site flanks and exhibited stable hydrogen bonds (Fig. 22).

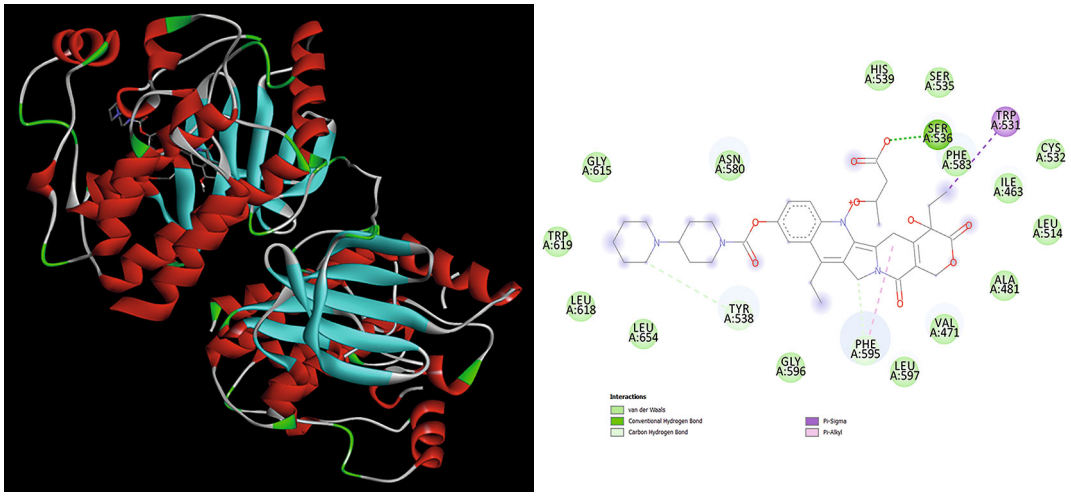

Fig. 19. Interaction of BRAF protein and molecule.

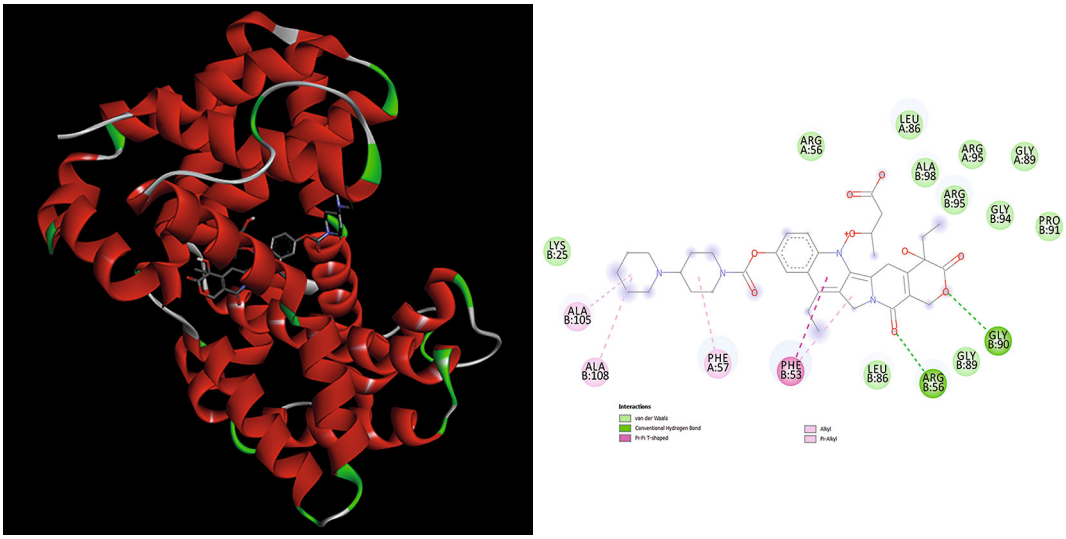

Fig. 20. Interaction of Bcl-w protein and molecule.

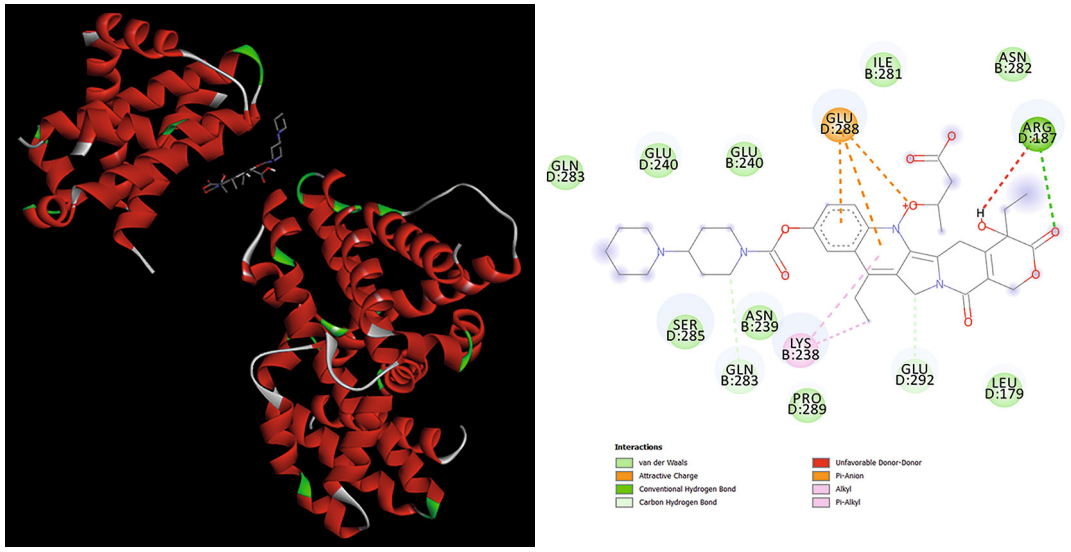

Fig. 21. Interaction of MCL-1 protein and molecule.

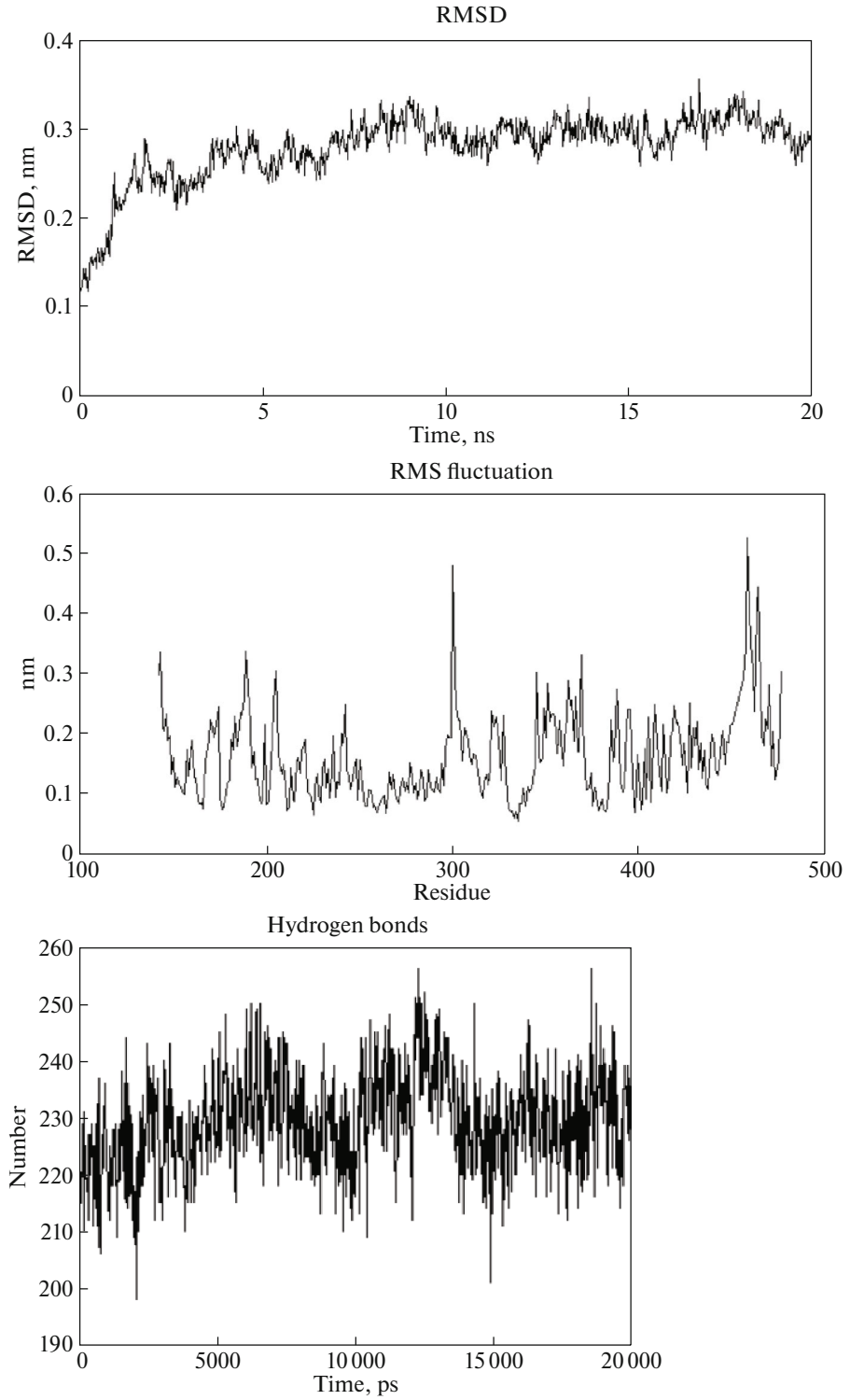

Fig. 22. Molecule dynamic results of AKT-1 protein and Irinotecan bound PHB coated nanoparticles.

4. CONCLUSIONS

In this study, Irinotecan loaded PHB coated magnetic nanoparticles were synthesized with targeted drug release for use in the treatment of cancers. We supported our study with theoretical data as well as experimental data. We analyzed the 3D drawings of the PHB molecule and the cancer drug Irinotecan with the GaussView program and optimized it with the Gaussian 09 program. Then, we created MEP maps

with the GaussView program to determine the binding regions of these structures. As a result of the conformations that bind the molecules from the determined regions, we determined the one with the lowest energy among them. We determined the newly formed bonds and the vibrational modes of these bonds.

Irinotecan was used as an anticancer agent and loaded on PHB-MNPs. To find the most efficient drug loading capacity on PHB-MNPs, we gradually increased the Irinotecan concentration and found the most efficient drug loading concentration to be 200 μg/mL. We also used molecular insertion studies to support cytotoxicity analyses. RMSD measurements gave an idea about conformational stability. Controlled Irinotecan release from PHB-MNPs appears to be a promising candidate for targeting cancer cells and overcoming drug resistance.

FUNDING

This work was supported by Kırşehir Ahi Evran University BAP coordinatorship (project no. FEF.A4.20.012).

CONFLICT OF INTEREST

The authors declare that they have no conflicts of interest.

REFERECES

1. S. Sarkar and M. Mandal, in *Breast Cancer: Focusing Tumor Microenvironment, Stem cells and Metastasis* (In-Tech Open, Rijeka, 2011).
2. J. Qin et al., Nano Life **9** (01n02), 1940003 (2019).
3. A. Aghebati-Maleki et al., J. Cell. Physiol. **235**, 1962 (2020).
4. N. Saeed, I. Hamzah, and S. Mahmood, J. Phys.: Conf. Ser. **1853**, 012061 (2021).
5. H. Gürsel, Nanopartiküller: Özellikleri ve Uygulama Alanları. https://shop.nanografi.com.tr/blografi/nanopartikuller-ozellikleri-ve-uygulama-alanlari/. Accessed 2022.
6. M. J. Ansari et al., BioNanoScience **12**, 627 (2022).
7. A. Farzin et al., Adv. Healthcare Mater. **9**, 1901058 (2020).
8. V. I. Shubayev, T. R. Pisanic II, and S. Jin, Adv. Drug Deliv. Rev. **61**, 467 (2009).
9. J. Maia, M. Santana, and M. Ré, Braz. J. Chem. Eng. **21** (1), 01 (2004).
10. L. Costa et al., in *Proceedings of the 2nd Brazilian Conference on Composite Materials, São Paulo, Brazil, 2014.*
11. U. Gunduz et al., Biomed. Pharmacother. **68**, 729 (2014).
12. L. R. Wiseman and A. Markham, Drugs **52**, 606 (1996).
13. M. J. Abraham, Rouhollah Khodadust, Gozde Unsoy, Immihan Ceren Garip, Zahide Didem Mumcuoglu, and Ufuk Gunduz, SoftwareX **1**, 19 (2015).
14. S. Yalcin, Rouhollah Khodadust, Gozde Unsoy, Immihan Ceren Garip, Zahide Didem Mumcuoglu, and Ufuk Gunduz, Synth. React. Inorg. Met.-Org. Nano-Met. Chem. **45**, 700 (2015). https://doi.org/10.1080/15533174.2013.831448
15. T. R. Sertbakan and F. Özçelik, J. Mol. Struct. **1250**, 131834 (2022).
16. RCSB PDB. https://www.rcsb.org. Accessed May 21, 2021.
17. PubChem. https://pubchem.ncbi.nlm.nih.gov. Accessed May 21, 2021
18. B. D. STUDIO, Comprehensive Modeling and Simulation for the Life Sciences. https://www.3ds.com/products-services/biovia/products/molecular-modeling-simulation/biovia-discovery-studio/. Accessed 2017.
19. WEBGRO. https://simlab.uams.edu/index.php. Accessed September 25, 2021.
20. S. Yalcin et al., Am. J. Therapeut. **21**, 453 (2014).
21. P. C. Babu et al., Spectrochim. Acta, Part A **98**, 1 (2012).
22. V. Rastogi et al., Spectrochim. Acta, Part A **58**, 1987 (2002).
23. G. Crippen et al., Nature (London, U.K.) **293**, 687 (1981).
24. L. Bellany, *The Infrared Spectra of Complex Molecules* (London, Chapman Hall, 1975), p. 1.
25. T. Göcen and M. H. Güven, Bilecik Şeyh Edebali Üniversitesi Fen Bilimleri Dergisi **7**, 553 (2020).
26. R. M. Silverstein and G. C. Bassler, J. Chem. Educ. **39**, 546 (1962).
27. P. M. Gill and P. von Rague Schleyer, J. Chem. Phys. **100**, 5066 (1994).
28. I. Fleming, *Frontier Orbitals and Organic Chemical Reactions* (Wiely, New York, 1976), p. 5.
29. D. Shindo and T. Oikawa, in Analytical Electron Microscopy for Materials Science (Springer, 2002), p. 81.
30. O. Trott and A. J. Olson, J. Comput. Chem. **31**, 455 (2010).
31. H. Bekker et al., in *Proceedings of the 4th International Conference on Computational Physics PC'92* (World Scientific, 1993).
32. C. Oostenbrink et al., J. Comput. Chem. **25**, 1656 (2004).
33. P. Bjelkmar et al., J. Chem. Theory Comput. **6**, 459 (2010).
34. K. Lindorff-Larsen et al., Proteins: Struct. Funct. Bioinform. **78**, 1950 (2010).